PAPER • **OPEN ACCESS**

Measurement uncertainty quantification for myocardial perfusion using cardiac positron emission tomography imaging

To cite this article: Ignacio X Partarrieu *et al* 2022 *Meas. Sci. Technol.* **33** 064002

OPEN ACCESS
IOP Publishing
Measurement Science and Technology
Meas. Sci. Technol. **33** (2022) 064002 (7pp)
https://doi.org/10.1088/1361-6501/ac58e3

Measurement uncertainty quantification for myocardial perfusion using cardiac positron emission tomography imaging

Ignacio X Partarrieu[1], Kavya Jagan[1], Andrew Fenwick[1], Chunlei Han[2], Reetta Siekkinen[2], Jarmo Teuho[2], Antti Saraste[2,3] and Nadia A S Smith[1,*]

[1] National Physical Laboratory, Hampton Road, Teddington, TW11 0LW, United Kingdom
[2] Turku PET Centre, Turku University Hospital and University of Turku, Turku 20520, Finland
[3] Heart Centre, Turku University Hospital, Turku 20520, Finland

E-mail: nadia.smith@npl.co.uk

Received 30 July 2021, revised 28 January 2022
Accepted for publication 25 February 2022
Published 17 March 2022

Abstract

Perfusion, the flow of blood, and hence oxygen, is essential to the functioning of the heart. Reduced perfusion (or ischemia), is a reliable indicator of the presence of significant obstructive coronary artery disease (CAD), which is one of the biggest causes of death in Europe. Myocardial perfusion imaging is a non-invasive technique used in the diagnosis, management and prognosis of CAD and is a key component in the triage of patients into treatment and non-treatment groups. Cardiac positron emission tomography (PET) is an imaging technique with high sensitivity and specificity to CAD, however perfusion measurements are difficult to calibrate against a common reference standard, and confidence in them is generally not quantified in terms of measurement uncertainty. There are a number of steps involved in measuring perfusion using cardiac PET—from patient preparation to data analysis—each associated with potential sources of uncertainty. The absence of measurement uncertainty quantification can lead to inaccuracies in measurement results, a lack of comparability between devices or scanning facilities, and is likely to be detrimental to a decision-making process. In this paper, we identify some of the sources of measurement uncertainty in the cardiac PET perfusion measurement pipeline. We assess their relative contribution by performing a sensitivity analysis using experimental data of a flow phantom acquired on a PET scanner. The results of this analysis will inform users of how parameter choices in their imaging pipeline affect the output of their measurements, and serves as a starting point to develop an uncertainty quantification method.

Keywords: cardiac PET perfusion, design of experiments, sensitivity analysis, sources of measurement uncertainty, flow phantom

(Some figures may appear in colour only in the online journal)

* Author to whom any correspondence should be addressed.

1. Introduction

Cardiovascular disease is a leading cause of mortality in Europe and is estimated to cost the European economy approximately €200 billion each year [1]. Perfusion, the flow of blood, and hence delivery to the capillary tissue, is essential to the functioning of the heart. Reduced perfusion, or ischemia, is an early marker of chronic heart disease [2].

Myocardial perfusion can be measured using positron emission tomography (PET) imaging, a non-invasive technique for the diagnosis, management and prognosis of cardiovascular disease. This technique reveals regions of underperfused myocardium, which are a reliable indicator of the presence of significant obstructive coronary artery disease (CAD). This imaging procedure is a key component in the triage of patients into treatment and non-treatment groups. Cardiac PET imaging offers a high sensitivity and specificity to CAD [3], however perfusion measurements are difficult to calibrate against a common reference standard due to complex acquisition and analysis protocols, and confidence in them is generally not quantified in terms of measurement uncertainty. The absence of measurement uncertainty quantification leads to a poorer understanding of measurement results and a lack of comparability between devices or scanning facilities. In clinical practice, the lack of evaluation of measurement uncertainty can ultimately lead to false diagnoses, patient distress, unnecessary treatments and litigation.

The measurement of cardiac perfusion using PET imaging is a complex process with many steps that range from patient preparation, through data gathering, to data analysis [4]. Each of these steps is associated with potential sources of measurement uncertainty. Left unaccounted for, these sources of uncertainty are likely to be detrimental to the measurement decision-making processes, affecting clinical outcomes. Uncertainty information can be used to quantify the risk of misclassification of patients [5], especially in borderline cases, which is a key difficulty in healthcare planning.

In this paper, we explore some of the sources of measurement uncertainty in the cardiac PET perfusion measurement pipeline and perform a sensitivity analysis to quantify their relative contribution. Experimental data of a flow phantom acquired on a PET scanner is used to carry out the sensitivity analysis, the results of which will inform users of how parameter choices in their imaging pipeline affect the output of their measurements. Furthermore, the analysis serves as a starting point to develop an uncertainty quantification method, which in turn will facilitate effective comparisons between the measuring systems used at different institutes.

This paper is structured as follows. Section 2 describes the measurement model, i.e. how to measure cardiac perfusion using PET imaging, as well as presenting the flow phantom used in this study and the experimental details. In section 3 the sensitivity analysis study is described and the results of it are presented. These results identify which of the investigated input parameters most affect the output of the measurements made. Section 4 discusses the main findings of the paper and section 5 presents a summary and thoughts on future direction of this work.

2. Cardiac PET perfusion measurements

PET is an imaging method for quantitatively measuring biochemical and physiological processes *in vivo* by using radio-pharmaceutical tracers—chemical compounds that are injected into the patient—and measuring the annihilation radiation path of such tracers using a coincidence detection technique, with counts typically quantified in Becquerels (Bq). PET tracers that are used for estimation of perfusion (or flow) include freely diffusible tracers such as [^{15}O]water (radiowater), partially extracted tracers including ^{82}Rb and [^{13}N]ammonia and, in the case of the myocardium, also [^{11}C]acetate. This section describes the measurement of flow using PET and [^{15}O]water, one of the most commonly used tracers for academic research, often considered the 'gold standard' PET perfusion measurement [3].

PET can be considered to be an inherently quantitative medical imaging method, provided that all the necessary data corrections (e.g. for attenuation, scatter and deadtime) and system calibrations (e.g. normalisation, conversion from counts to Bq and system geometry) are performed correctly. Each voxel in a reconstructed time series of PET images represents the concentration of radioactivity (Bq ml^{-1}) as a function of time in minutes (min), from which time-activity-curves (TACs) can be extracted. Values of perfusion based on PET images are generally given in units of ml (g min)$^{-1}$, and can be derived by performing kinetic modelling [6–10] of TACs measured from the blood pool and myocardial tissue.

A basic image acquisition and data analysis procedure for a typical radiowater PET perfusion study involves the following steps: (a) preparation and injection of the radiowater into patient (or test object), (b) image acquisition, (c) image reconstruction, (d) post-processing of the reconstructed images and (e) data analysis to calculate the flow. Figure 1 shows a schematic representation of each of these steps with associated sources of uncertainty for each one.

2.1. Flow phantom

In order to fully understand and control the sources of uncertainty involved in the measurement process as shown in figure 1, a flow phantom (DCE Dynamic Flow Phantom, Shelley Medical Imaging Technologies, Canada) was used in a similar way to [11] , and a schematic of the set up is shown in figure 2. Phantom validation for cardiac PET perfusion imaging is presented in [12].

The phantom set-up contains a water container, a peristaltic pump, an injection port, a phantom shell, a flow constrictor valve and flow meters. A schematic of the flow phantom is shown in figure 2. The input chamber models the left ventricle blood pool whereas the exchange cylinder and perforated tube model tracer exchange in myocardial tissue. These allow to measure input and tissue TACs for kinetic modelling in a similar fashion to what is done with patient data.

The model used to calculate flow rate in the phantom is given by equation (1) [12]:

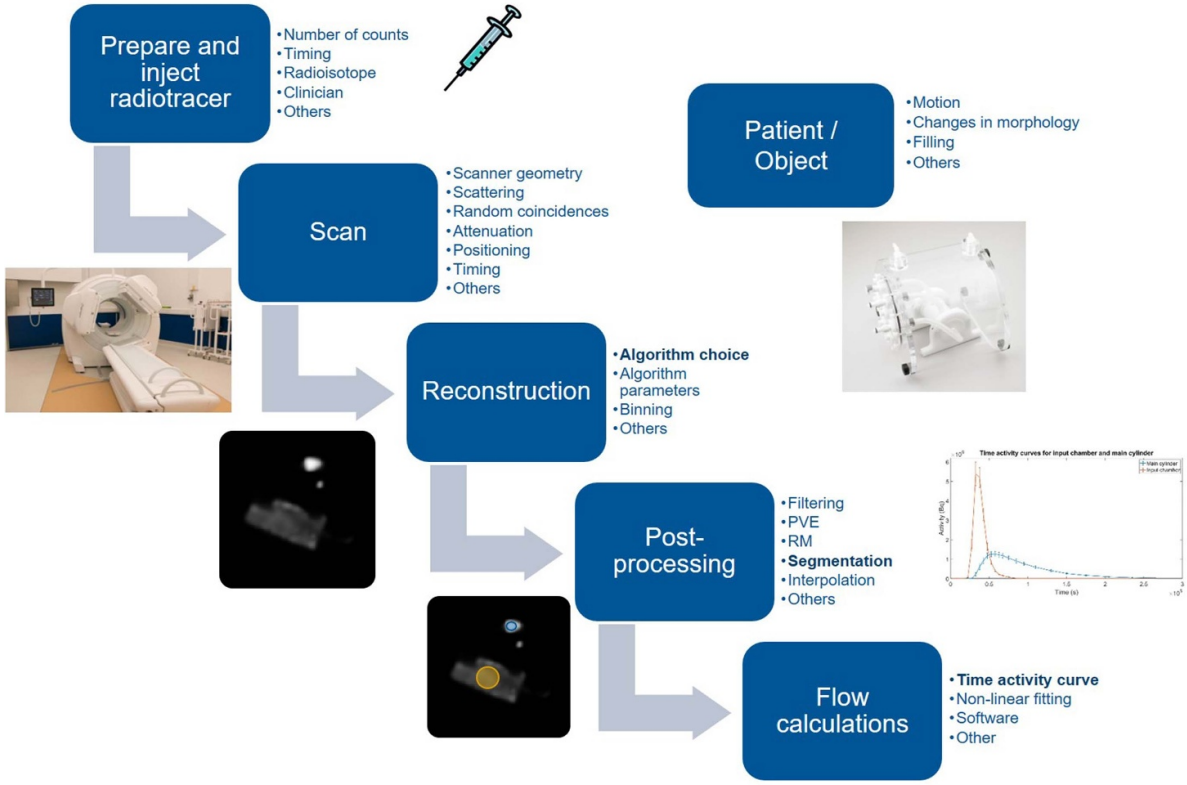

Figure 1. Schematic description of the PET measurement pipeline steps to estimate flow with associated sources of uncertainty for each one. Steps highlighted in dark blue are the subset examined in this paper.

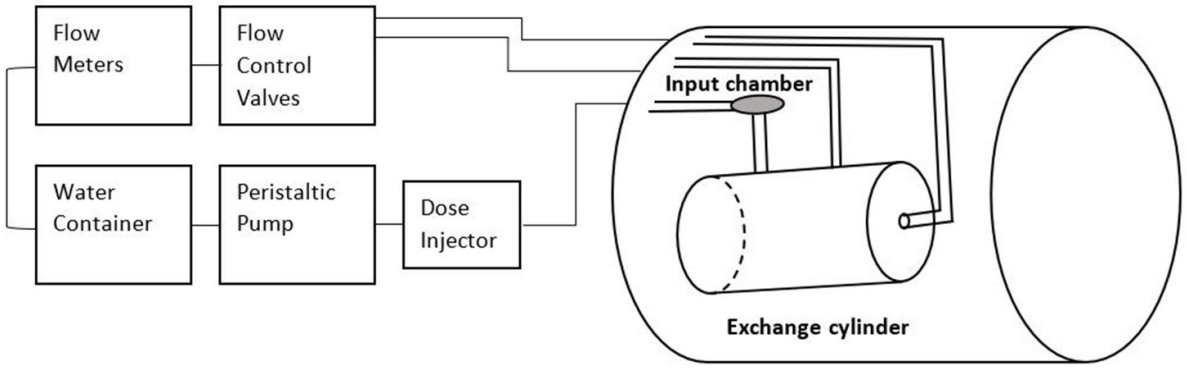

Figure 2. Schematic (not to scale) of the DCE dynamic flow phantom. Water is run from the container by the peristaltic pump to the phantom in a closed-loop cycle. Radiotracer is injected through the port labelled dose injector. This is run through the input chamber to a perforated tube inside the exchange cylinder. Flow inside the perforated tube and the exchange cylinder are constricted with flow valves and measured with flow meters.

$$C_{\text{cyl}}\text{VOI}(t) = (1 - \text{ISF}) \times C_{\text{input}}\text{VOI}(t - \text{delay}) + \text{ISF} \times q_{\text{in}} \times e^{-q_{\text{out}} \times t} * C_{\text{input}}\text{VOI}(t - \text{delay}) \quad (1)$$

where $C_{\text{cyl}}\text{VOI}(t)$ is the activity concentration in the cylinder (Bq ml^{-1}) volume of interest (VOI) at time t (min) after injection, $C_{\text{input}}\text{VOI}(t - \text{delay})$ is the activity concentration in the input chamber VOI (Bq ml^{-1}) with a 'delay' (min) which must be assessed, 'ISF' is the input signal fraction (equivalent to the fractional blood volume) to account for signal spillover and q_{in} and q_{out} are wash in and wash out rates (min^{-1}), which can be converted to absolute flow values (ml min^{-1}) through multiplication by the total volume of the cylinder. $*$ denotes a convolution.

$C_{\text{cyl}}\text{VOI}(t)$ and $C_{\text{input}}\text{VOI}(t - \text{delay})$ can be calculated from the TACs by multiplying their time point values by the VOI volume and dividing the result by the exchange cylinder (160 ml) and input chamber (15.7 ml) volumes, respectively. With these, we can then solve for the four parameters: 'delay', 'ISF', q_{in} and q_{out} using a non-linear least squares fitting approach [13].

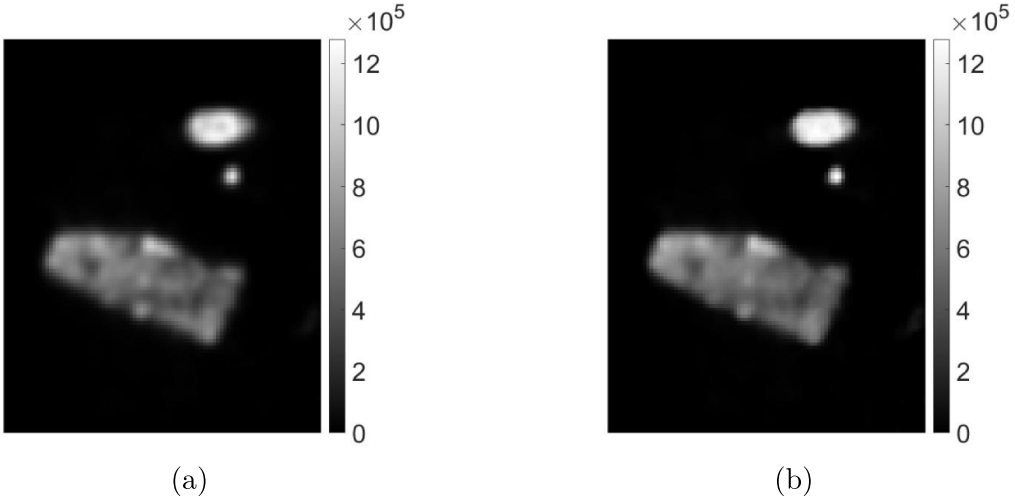

Figure 3. Single slice images of (a) a 3D-OSEM reconstruction (b) a BSREM reconstruction, both of the same acquisition which had a 200 ml min^{-1} flow rate with 20% flow in the exchange cylinder. The bright, uppermost point is the input chamber and the largest object, located in the bottom, is the exchange cylinder.

2.2. Experimental acquisition details

The flow phantom was scanned on a digital Discovery MI PET/CT system (DMI, GE Healthcare, Milwaukee, US) after injection of a target 500 MBq of [^{15}O]water. Acquisition parameters were fixed for each measurement. Three measurements were carried out after each injection, where the flow through the phantom was increased from 150 ml min^{-1} to 250 ml min^{-1} in steps of 50 ml min^{-1}, with a consistent percentage of the flow 'lost' to tracer exchange, which is later referred to as "Flow percentage". Once acquired, two images were reconstructed using:

- a three dimensional ordered subset expectation maximization (3D-OSEM) using point spread function modelling and time of flight with a 5 mm Gaussian post-filter and a 35 cm field of view.
- and a block sequential regularized expectation maximization (BSREM) with a beta-value of 350.
- Both reconstruction algorithms were run for three iterations and 16 subsets, using a matrix size of 192 by 192.

Single time-point examples of these reconstructions may be seen in figure 3. It can be seen that BSREM images are smoother than OSEM images. The resulting images then had two volumes of interest defined: one over the input chamber and one over the exchange cylinder, with the volumes varied over representative ranges.

3. The effect of input parameters on the perfusion measurement

3.1. Design of experiments

In order to determine how various factors in the perfusion measurement pipeline contribute to the variability of $C_{\text{cyl}}\text{VOI}(t)$ and $C_{\text{input}}\text{VOI}(t-\text{delay})$ measurements, which are the key inputs for the kinetic modelling equation, we performed a full factorial experiment measuring the flow phantom. The levels taken by all factors may be found in table 1.

Table 1. List of factors examined during experimentation and their levels. The ranges selected are representative of clinical values.

Factor	Levels
Flow rate (ml min^{-1})	150, 200, 250
Flow percentage (%)	20, 40, 60, 80
Input chamber VOI (ml)	1, 2, 3, 4, 5
Exchange cylinder VOI (ml)	5, 10, 15, 20, 25, 30, 35, 40, 45, 50
Reconstruction algorithm	BSREM, OSEM

This design resulted in 1200 VOIs drawn for the input chamber and exchange cylinder respectively, from which the TACs were extracted (e.g. figure 4). These were used to obtain the $C_{\text{cyl}}\text{VOI}(t)$ and $C_{\text{input}}\text{VOI}(t-\text{delay})$ concentration curves, from which in turn we calculated the areas under the curves (AUC) $\text{AUC}_{C_{\text{cyl}}}$ and $\text{AUC}_{C_{\text{input}}}$ as representative summary statistics. The VOIs were centered on the input and exchange cylinders respectively using an automated algorithm that detected the two largest areas of activity in the image, and the volumes taken selected based on clinical VOI data gathered by the clinicians.

3.2. Sensitivity analysis

In order to determine the sensitivity of $\text{AUC}_{C_{\text{cyl}}}$ and $\text{AUC}_{C_{\text{input}}}$ to factors in the processing pipeline, the 1200 results of the full factorial experiment were processed using analysis of variance (ANOVA), which calculates the sum of squares SS_A due to each factor or factor interaction A [14]. Phantom flow rate, flow percentage, exchange cylinder VOI, input chamber VOI and reconstruction type were all varied as per table 1, taking all possible combinations of the values therein. The sum of

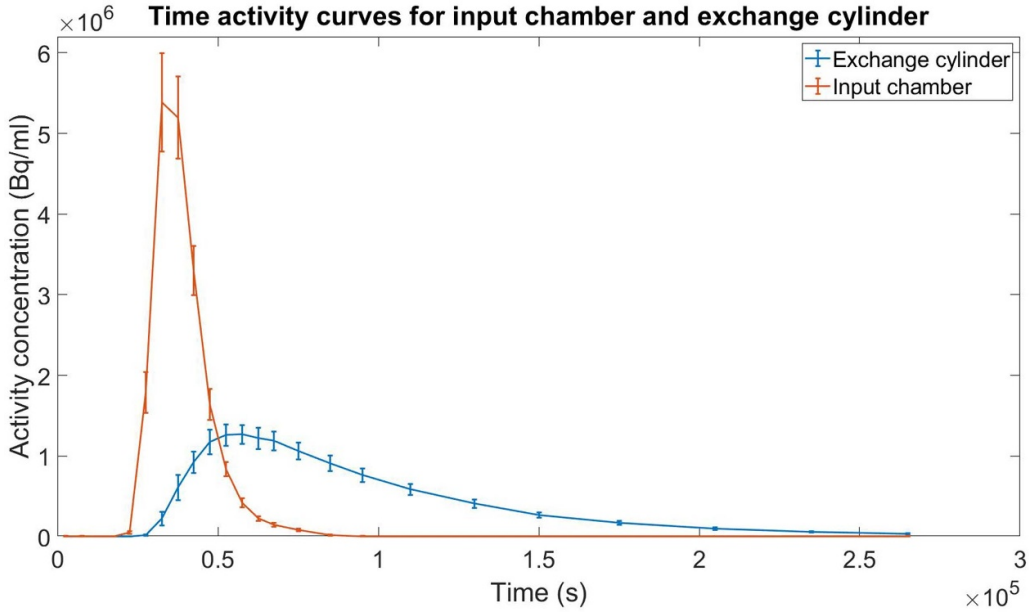

Figure 4. Input chamber and exchange cylinder time activity curves. Each data point represents the average value within the corresponding VOI. The error bars are the standard deviation within the VOI, with a half length being equal to σ. It can be seen that the activity concentration peak for the input chamber is larger than for the exchange cylinder.

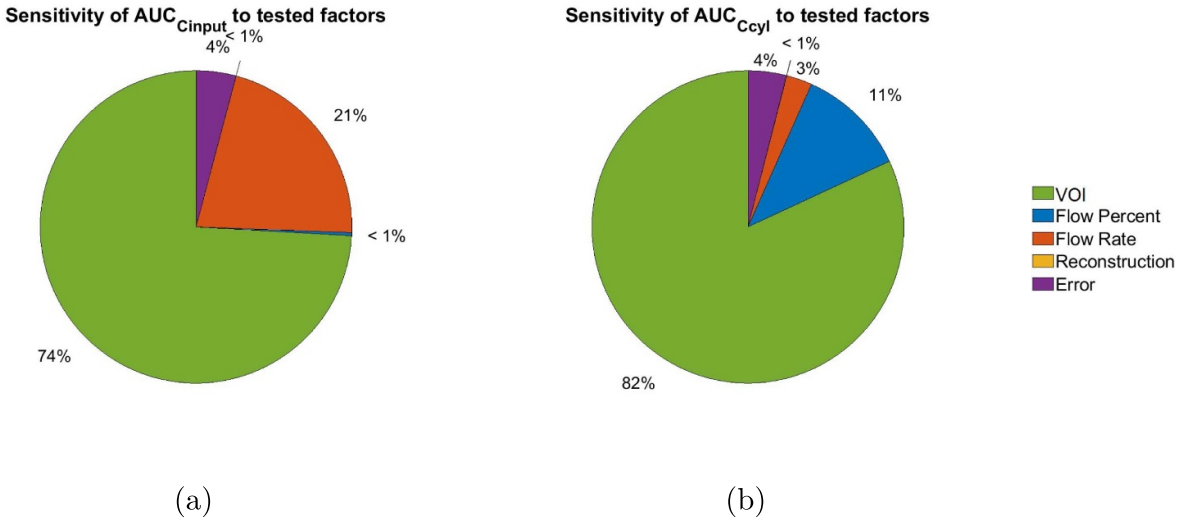

Figure 5. Pie charts showing the sensitivity of the input chamber and cylinder concentration curve AUCs to the factors investigated.The legend is shared, with VOI referring specifically to the respective volume (either input chamber or exchange cylinder). It can be seen that activity curves are most sensitive to the VOI (74% and 82% respectively), followed by flow rate (21%) for the $\mathrm{AUC}_{C_{\mathrm{input}}}$ and flow percent (11%) for the $\mathrm{AUC}_{C_{\mathrm{cyl}}}$. The error accounts for 4% of the sensitivity for both.

squares contributions of these factors and their interactions were then compared to the total sum of squares SS_T, in order to calculate Pearson's η^2 coefficient [15]:

$$\eta_A^2 = \frac{\mathrm{SS}_A}{\mathrm{SS}_T}. \tag{2}$$

This coefficient describes the relative variation in the dataset and provides an indication of which factors affect the calculated concentration AUCs the most, with η^2 taking larger values for these. By definition, this should be a combination of the VOI and the true underlying flow rate for the input chamber, or the VOI and both the true flow rate and flow percentage for the exchange cylinder. In a full factorial experiment, values of η^2 sum to one.

3.3. Results of the sensitivity analysis

In figure 5, the η^2 values have been converted to percentages. The term 'error' encapsulates all interactions between the factors investigated. From this figure, it is possible to see that the calculation of $\mathrm{AUC}_{C_{\mathrm{cyl}}}$ and $\mathrm{AUC}_{C_{\mathrm{input}}}$ are both strongly affected by changes in the VOI over the ranges investigated,

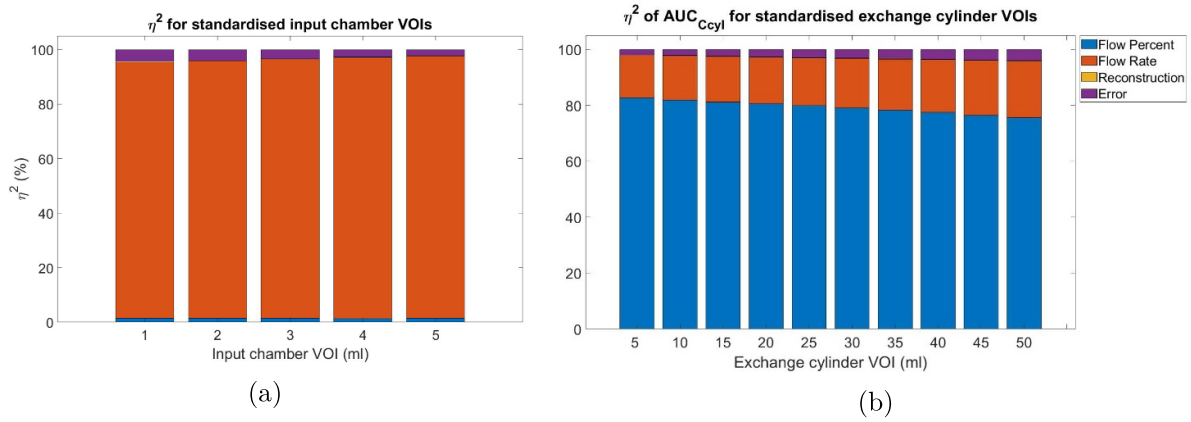

Figure 6. Bar charts showing the sensitivity of the input chamber and cylinder TAC AUCs to the factors investigated once VOI is standardised. The legend and y axis label are shared. For the AUC$_{C_{\text{input}}}$, sensitivity to the flow percent is negligible whereas it is approximately 80% for the AUC$_{C_{\text{input}}}$ for all investigated volumes. Sensitivity to the flow rate is approximately 95% for the AUC$_{C_{\text{input}}}$, and hovers around 20% for the AUC$_{C_{\text{cyl}}}$. The effect of the reconstruction term is negligible.

which is to be expected given their definitions. Flow rate is the second most important factor investigated for AUC$_{C_{\text{input}}}$, whereas it is flow percentage for AUC$_{C_{\text{cyl}}}$. As the VOI was an important factor, we thought it would be valuable to further investigate if specific VOIs resulted in improved sensitivity of the concentration value to the flow factors. The results may be seen in figure 6.

In figure 6, we can see that standardisation of the VOI for the AUC$_{C_{\text{input}}}$ leads to flow rate becoming the dominant factor, and the specific volume has a minor effect. For the AUC$_{C_{\text{cyl}}}$, the dominant factor becomes the flow percentage, with the specific volume again having a minor effect, where as the VOI gets larger sensitivity to the flow percentage reduces by approximately 6%, with sensitivity to flow rate and error both increasing.

4. Discussion

In this paper we have outlined the need for an improved understanding of how cardiac PET measurements are affected by factors in the measurement pipeline. Using AUC$_{C_{\text{cyl}}}$ and AUC$_{C_{\text{input}}}$ as representative summary statistics, we have shown that VOI standardisation is important for measurements of the exchange cylinder and input chamber. In this latter scenario, flow percentage was the dominant factor, as expected. We also observed a meaningful contribution from flow rate to the sum of squares, which increased for larger VOIs. However, this effect is small and additional data should be gathered before making claims of significance. The reconstruction algorithm effect was negligible. This could be due to the fact that the algorithms were run to result in equivalent voxel sizes, and that in this case, the BSREM algorithm was run to have similar noise and resolution properties as the OSEM algorithm. Varying algorithm sub-parameters may lead to the reconstruction's η^2 contribution increasing.

Kinetic flow values of the phantom were not modelled from the TACs for this paper, but would be of value in future analyses as we would expect their sensitivity to reflect those of the AUCs calculated. Additionally, it should be noted that although modelling kinetics on a phantom provides valuable insight into model appropriateness and sensitivity, the phantom is highly idealised. In actual patient scans the location of the 'input chamber' and 'exchange cylinder' equivalents are less clearly defined, tissue spill-over effects are present which can confound the analysis and patient motion results in lower quality images. Due to these factors, the kinetic model to be used varies from the one used for the phantom.

The sensitivity analysis here addresses a few initial factors in the perfusion quantification pipeline. Many other factors exist, and some may contribute significantly to the outcome. It is important to methodologically determine which factors are likely to be important contributors to final measurement results in order to be able to suggest appropriate measures for standardisation. Future work will expand upon the analysis seen here to additional parameters, guided by clinical concerns.

5. Concluding remarks and future work

This initial work demonstrates the importance of properly assessing the sensitivity of a imaging pipeline to the factors being investigated. Using a sensitivity analysis, we have identified the main contributors to the total sum of squares of the data and proposed standardisation schemes. We have also shown that reconstruction effects are negligible for AUC calculations.

We plan on further propagating this analysis through to the final flow values as opposed to only analysing the AUC as well as investigating additional factors in the PET perfusion pipeline, to see how initial input variations affect the end perfusion results, with the end goal of establishing optimal factor levels for flow measurements.

After that we plan on quantifying the uncertainty due to each of these factors in the perfusion pipeline using a Monte Carlo method. The sensitivity analysis carried out here will guide the choice of input quantities into the uncertainty

quantification method and help assign distributions to them based on expert knowledge.

All these steps contribute towards the project's end goal of being able to establish traceability of PET perfusion measurements and quantify uncertainties through the traceability chain, which will enable standardisation across scanners and centres.

Data availability statement

The data that support the findings of this study are available upon reasonable request from the authors.

Acknowledgments

This project 19SIP04 TracPETperf has received funding from the European Metrology Research Programme (EMPIR) co-financed by the Participating States and from the European Union's Horizon 2020 research and innovation programme. This paper reflects only the authors' view and EURAMET is not responsible for any use that may be made of the information it contains. This study was also supported by a grant from the Instrumentarium Science Foundation in Finland.

ORCID iDs

Ignacio X Partarrieu https://orcid.org/0000-0002-5862-1462
Kavya Jagan https://orcid.org/0000-0002-3531-3029
Nadia A S Smith https://orcid.org/0000-0002-6503-3001

References

[1] Timmis A *et al* 2020 European Society of Cardiology: cardiovascular disease statistics 2019 *Eur. Heart J.* **41** 12–85
[2] Shaw L J *et al* 2008 Optimal medical therapy with or without percutaneous coronary intervention to reduce ischemic burden *Circulation* **117** 1283–91
[3] Moody J B, Lee B C, Corbett J R, Ficaro E P and Murthy V L 2015 Precision and accuracy of clinical quantification of myocardial blood flow by dynamic PET: a technical perspective *J. Nucl. Cardiol.* **22** 935–51
[4] Knuuti J *et al* 2020 2019 ESC Guidelines for the diagnosis and management of chronic coronary syndromes *Eur. Heart J.* **41** 407–77
[5] Jagan K *et al* 2021 Using measurement uncertainty in a risk-based decision-making framework for clinical diagnosis *Advanced Mathematical and Computational Tools in Metrology and Testing XII* vol 90 ed F Pavese, A B Forbes, N F Zhang and A G Chunovkina Series on Advances in Mathematics for Applied Sciences (Singapore: World Scientific) pp 306–21
[6] Araujo L I *et al* 1991 Noninvasive quantification of regional myocardial blood flow in coronary artery disease with oxygen-15-labeled carbon dioxide inhalation and positron emission tomography *Circulation* **83** 875–85
[7] Hermansen F, Rosen S D, Fath-Ordoubadi F, Kooner J S, Clark J C and Camici P G 1998 Measurement of myocardial blood flow with ^{15}O labelled water: comparison of different administration protocols *Eur. J. Nucl. Med.* **25** 751–9
[8] Iida H, Rhodes C G, de Silva R, Yamamoto Y, Araujo L I and Maseri A 1991 Myocardial tissue fraction—correction for partial volume effects and measure of tissue viability *J. Nucl. Med.* **32** 2169–75
[9] Iida H, Rhodes C G, de Silva R, Araujo L I, Bloomfield P M and Lammertsma A A 1992 Use of the left ventricular time-activity curve as a noninvasive input function in dynamic ^{15}O-water positron emission tomography *J. Nucl. Med.* **33** 1669–77
[10] Watabe H, Jino H, Kawachi N, Teramoto N, Hayashi T and Ohta Y 2005 Parametric imaging of myocardial blood flow with ^{15}O-water and PET using the basis function method *J. Nucl. Med.* **46** 1219–24
[11] Siekkinen R *et al* 2020 Study of the effect of reconstruction parameters for myocardial perfusion imaging in PET with a novel flow phantom *Front. Phys.* **8**
[12] Gabrani-Juma H *et al* 2017 Validation of a multimodality flow phantom and its application for assessment of dynamic SPECT and PET technologies *IEEE Trans. Med. Imaging* **36** 132–41
[13] Siekkinen R *et al* 2021 Assessment of a digital and an analog PET/CT system for accurate myocardial perfusion imaging with a flow phantom *J. Nucl. Cardiol.* (https://doi.org/10.1007/s12350-021-02631-9)
[14] Miller J and Haden P 2006 Statistical analysis with the general linear model *Creative Commons Attribution*
[15] Cohen J 1973 Eta-squared and partial eta-squared in fixed factor ANOVA designs *Educ. Psychol. Meas.* **33** 107–12